Polymer 51 (2010) 4928–4936

Contents lists available at ScienceDirect

Polymer

journal homepage: www.elsevier.com/locate/polymer

Unconfined fluid electrospun into high quality nanofibers from a plate edge

Nagarajan Muthuraman Thoppey [a], Jason R. Bochinski [b], Laura I. Clarke [b,**], Russell E. Gorga [a,*]

[a] Fiber and Polymer Science Program, North Carolina State University, Raleigh, NC 27695, USA
[b] Department of Physics, North Carolina State University, Raleigh, NC 27695, USA

ARTICLE INFO

Article history:
Received 8 June 2010
Received in revised form
27 July 2010
Accepted 31 July 2010
Available online 14 August 2010

Keywords:
Nanofibers
Scaling-up production
Needle-less electrospinning

ABSTRACT

We demonstrate an easily-implemented, edge-plate geometry for electrospinning and produce high quality nanofibers from unconfined polymer fluids. We show that for electrospinning in general, the electric field gradient, not just the electric field amplitude, is a critical parameter for successful self-initiated jetting. Considering a single spinning site, the edge-plate configuration resulted in the same or a higher fabrication rate as traditional needle electrospinning, while producing nanofibers similar in quality (diameter, diameter distribution, and collected mat porosity); moreover, this novel configuration operates without the possibility of clogging and has high potential for scale-up. We analyze the fundamental physical processes which underlie edge-plate electrospinning, including electric field, working distance, and feed rate dependence and the resultant changes to the linear and whipping regions, and thus to the fiber diameter. We conclude that the edge-plate configuration functions in a remarkably similar manner to traditional needle electrospinning.

© 2010 Elsevier Ltd. All rights reserved.

1. Introduction

Needle electrospinning is a common, simple, and versatile technique for nanofiber fabrication [1–6], applicable to a wide range of polymers with limited capital investment. Nanofibers from 10 to 1000 nm in diameter can be readily produced from polymer solutions or melts and collected as nonwoven mats having ~70% porosity. These fibers can be randomly coated directly onto a variety of pre-existing structures such as an air filter or a garment, or generated with spatial alignment. Electrospun nanofibers have significant technological promise both due to their high surface area to volume ratio (e.g., for catalysis [1]) and because the collected nanofibrous mats are lightweight due to their high porosity. The porosity and micro-scaled pore size provide good filtration efficiency, enabling applications in the liquid and air filtration industry [7]; the nanofibers' size and mat porosity are also well-suited for medical applications, such as tissue scaffolding, drug delivery, and wound protection [8,9]. In addition, nanofibrous scaffolds doped with conductive particles have been shown to perform as strain sensors [10].

Electrospinning in its most well-known implementation utilizes a large electric potential difference applied between an electrically-charged, conducting needle, through which fluid is pumped by a syringe pump, and a flat collector plate (Fig. 1): we refer to such a needle-plate (source–collector) arrangement as traditional needle electrospinning (TNE). The polymer solution emerging from the needle is charged and electrostatic forces propel the fluid through the spatially inhomogeneous electric field towards the grounded collector plate. Under suitably optimized conditions (e.g., polymer concentration, electric field magnitude and distribution, and solution feed rate), the jet follows a linear path for a short distance from the tip of the needle and then becomes unstable, resulting in a whipping region where the solvent evaporates as the fiber is elongated and its diameter reduced. This action produces solvent-free polymer nanofibers randomly deposited on the collector plate, commonly being a few hundred nanometers in diameter.

Despite the utility of these nanostructured materials, widespread industrial implementation of electrospun nanofibers is primarily limited by low fabrication rates (0.01–0.1 g/hr) [11] in the TNE configuration, where the nanofiber source is a single jet arising from a needle aperture through which the polymer solution is expelled. Numerous approaches to scaling-up the fabrication rate of electrospun materials [12] have been reported; these techniques can be summarized as 1) spinning from multiple apertures, 2) generating multiple jets from a given aperture, or 3) generating jet sites without apertures [13,14].

In general, these previously reported approaches to scale-up electrospinning can be classified based on the manner in which the solvent solution is dispensed, as using either a confined or unconfined fluid-volume feed method. In confined feed systems,

* Corresponding author. Fiber and Polymer Science Program, North Carolina State University, Raleigh, NC 27695, USA. Tel.: +1 919 515 6553; fax: +1 919 515 6532.
** Corresponding author. Tel.: +1 919 513 7359; fax: +1 919 515 6538.
E-mail addresses: liclarke@ncsu.edu (L.I. Clarke), regorga@ncsu.edu (R.E. Gorga).

0032-3861/$ – see front matter © 2010 Elsevier Ltd. All rights reserved.
doi:10.1016/j.polymer.2010.07.046

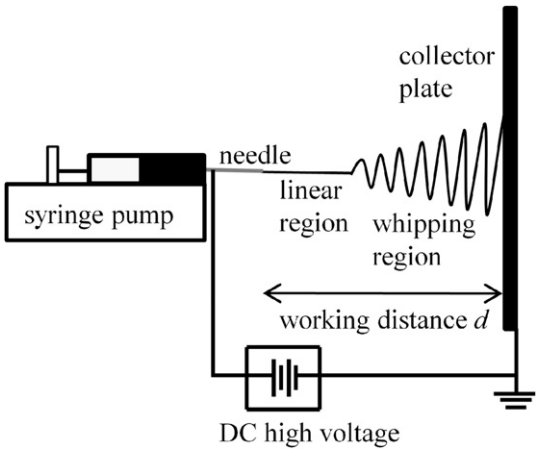

Fig. 1. A traditional needle electrospinning apparatus (TNE).

the polymer solution is typically injected at a constant rate (save for a few approaches which are gravity-assisted [15]) into an enclosed capillary (such as a needle or nozzle). Most confined feed systems utilize one or more nozzles [16–25] and each nozzle can produce one or more polymer jets, with additional jets formed by use of a grooved tip [26], a curved collector [27], or jet splitting [28]. Additional confined feed systems involving different types of enclosures continue to emerge in the literature and are summarized in a recent review [12]; these include the use of porous tubes with random and linear holes [11,29], conical wire coils with openings between the wires [15], multiple plastic tips where high voltage is applied directly to the polymer through a submerged electrode [30], a rotating cylindrical spinning head with extrusion tubes [31], a multi-channel microfluidic device [32], and electrospinning using charge injection [33]. We note that the majority of approaches to increase throughput in electrospinning previously reported in the literature utilize multiple nozzles with confined feed and hence, are essentially a linear scale-up of TNE.

One of the major advantages of the confined feed approach is the restricted flow rate, which is important for maintaining a continuous stable electrospinning process and controlling the nanofiber diameter in order to produce narrow diameter, high quality fibers, as higher flow rates are generally associated with thicker fibers. However, confined feed systems are also innately prone to clogging, and typically require an engineered structure for each jet (or several jets), thus significantly increasing system complexity. Conversely, in unconfined feed systems, a polymer solution usually flows unconstrained over the surface of another material. Examples of such unconfined feed approaches include spinning from a polymer solution coating a metallic fluid in the presence of magnetic and electric fields (which generates spike-like structures [14]), spinning from the rotating cylindrical solid surface in the Nanospider™ [13], cleft electrospinning [34], bubble electrospinning [35], and centrifugal electrospinning [36]. The advantage of utilizing unconfined flow is the ability to form, in principle, more jets without any highly engineered parts that may require maintenance. Detriments commonly resulting from unconfined feed systems are the production of larger diameter fibers and a broader distribution of fiber diameters. Thus, with the benefit of increased throughput, the fiber quality is often negatively impacted.

In this work we demonstrate an unconfined feed system that combines the advantages of both aforementioned approaches, resulting in fiber quality that is similar to TNE while having the potential for significant scale-up without system complexity. In order to study and understand the electrospinning process in an aperture-free system, the edge of a flat plate has been used as a source electrode onto which polymer solution is placed as droplets or undergoes a gravity-assisted flow. This simple geometry provides information about the particular challenges and opportunities generally present in unconfined feed systems. Our proposed system provides a strong and relatively inhomogeneous electric field (i.e., possessing a significant gradient in the electric field magnitude along the spinning axis) compared to other unconfined approaches on flat surfaces, but without the additional engineering complexity of forming sharp needle-like structures to imitate the TNE geometry.

Nanofibers possessing similar fiber diameter and diameter distributions were successfully fabricated while operating at comparable voltages and working distance as those from an aperture-based system, yet with more intrinsic flexibility to potentially scale-up the process without openings or nozzles that could potentially clog. The field gradient (the rate of change in the electric field magnitude along the spinning axis) at the site of jet formation is important; in particular, the relatively homogeneous electric field near the plate center does not promote electrospinning as compared with the significantly more spatially inhomogeneous field at the needle tip in the needle-plate configuration. However, the strong field gradient at the plate edge similarly allows electrospinning from unconfined droplets of the polymer solution and formation of fibers with diameters and distributions similar to those fabricated by TNE for the same polymer solution. Furthermore, this methodology is extendable to systems with many "edges" for massively-parallel electrospinning, that is, significantly higher throughput. We report a detailed examination of the changes in fiber diameter, diameter distribution, and mat porosity as a function of the electric field magnitude and geometry, and conclude that the process is quite stable over a range of experimental conditions. The connection between fiber properties and spinning conditions via changes in the length and duration of the linear region and the degree of whipping is discussed in the context of comparing plate edge and traditional needle electrospinning. Not only do these results address issues specific to such a surface-based, parallel, unconfined feed, aperture-less electrospinning approach, they also continue to expand understanding of electrospinning in general terms.

2. Experimental

2.1. Materials

Except where noted, polyethylene oxide (PEO) in water was used for all experiments. PEO with an average molecular weight of 400,000 g/mol (Scientific Polymer Products) was used without further purification. Solutions of 6 weight-percent (wt%) polymer in de-ionized water were stirred for 24 hr at room temperature to aid dissolution; in some experiments, Rhodamine 590 chloride (R6G) (Exciton) (0.001 wt%) was added to PEO solutions in order to enhance imaging contrast when viewing the electrospinning process. Additionally, for a single experiment polycaprolactone (PCL) having an average molecular weight between 70,000 and 90,000 g/mol (Scientific Polymer Products) was also used as received. Solutions of 12 wt% PCL in equal parts dichloromethane (DCM) and dimethylformamide (DMF) (Sigma Aldrich) were stirred for 3 hr at room temperature and used as discussed in Section 3.2.

The source plates were chemically treated with silanes containing a hydrophobic terminal group (decyltrichlorosilane (C_{10})) (Sigma Aldrich), forming self-assembled monolayers (SAMs) on the native oxide layer of the plate surface, in order to chemically-modify the

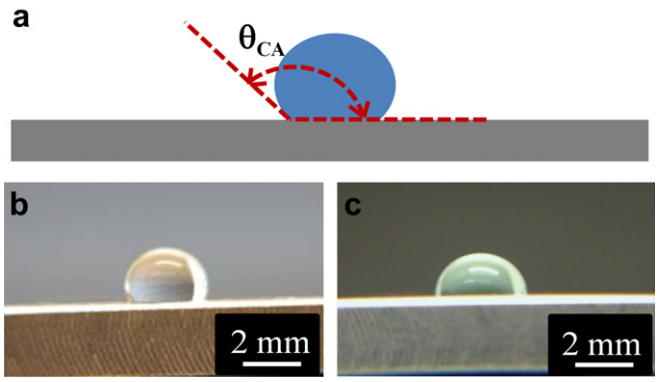

Fig. 2. (a) Schematic of contact angle (θ_{CA}) measurement. Contact angle measurements on an aluminum plate whose wettability has been chemically-modified by treatment with C_{10} for a droplet of (b) water (105 ± 3°), and (c) 6 wt% PEO:water spinning solution (87 ± 3°).

source plate and reduce surface interactions between the water-based polymer solution and the plate [37]. The aluminum source plates (McMaster-Carr) ((length × width × thickness) 12" × 8" × 1/4" for the parallel-plate geometry, and 4" × 1½" × 1/16" for both the edge-plate and multi-source plate configurations) were cleaned in a UV-ozone cleaner for 30 min to enhance the number of available hydroxyl groups for the film growth reaction and ensure suitable surface cleanliness. The plates were preheated in an oven for 30 min at 90 °C then exposed to C_{10} vapor for 60 min. During this process, the hydroxyl surface groups react with the alkyltrichlorosilanes, forming a covalently-bound, disordered [38] alkylsiloxane monolayer with a hydrophobic methyl and methylene-terminated surface [39]. Plates were rinsed with methanol for 10 s and sonicated in toluene for 10 min to remove any polymerized material not permanently attached to the surface. This film growth procedure provides a hydrophobic monolayer-like coating on the metal plate. Water contact angle θ_{CA} (Fig. 2a) (droplet size 2 μl, average of five readings) increased from ~0° measured before film growth (i.e., the water wetted the surface) to 105 ± 3° (Fig. 2b) after treatment. For the PEO:water solution used for electrospinning, the contact angle on the hydrophobic coating was 87 ± 3° (Fig. 2c). The contact angle of the PCL solution on both treated and un-treated (clean) plates was similar, ~20°. Aluminum collector plates (15" × 12" × 1/8") (McMaster-Carr) were used without further treatment, where aluminum foil typically covered the plate in order to collect the electrospun mat samples for further measurements.

2.2. Apparatus

For the TNE experiments, a programmable, syringe pump (New Era Systems, Model No. NE-1000) with a 5 ml plastic syringe controllably injected the polymer solution through a 4" stainless steel (size 20 or size 14 gauge) needle (Sigma Aldrich). A power supply (Glassman High Voltage, Model No. FC60R2) provided positive-polarity, high voltage to the needle (or source plate in the plate electrospinning configurations) while the collector plate was held at ground potential. Polymer solution viscosity measurements were performed (REOLOGICA Instruments AB, Stresstech) at 25 °C for the PEO (PCL) solution, determining a value of 9250 cP (170 cP). A camcorder (Panasonic, Model SDR–H60) with a 6 mm × 18 mm T monocular (Zeiss) recorded images while the polymer jets were continuously illuminated with industrial video lighting equipment (Olympus).

In all configurations discussed, we refer to the working distance d as the minimum spatial separation between the source object (usually the location of initiation of spinning) and collector surface. As discussed later, we utilize traditional needle-plate electrospinning under what we refer to as typical (TNE), as well as extended (TNE*), working distances; for typical (or sometimes also called optimal) TNE, d is 15 cm and the applied voltage is 11 or 15 kV; for extended needle-plate spinning (TNE*), d is 35 cm and the applied voltage is increased to 28 kV. Three alternative configurations in addition to TNE were utilized for electrospinning, as depicted in Fig. 3. The parallel-plate arrangement consisted of identical plates oriented horizontally with one placed directly

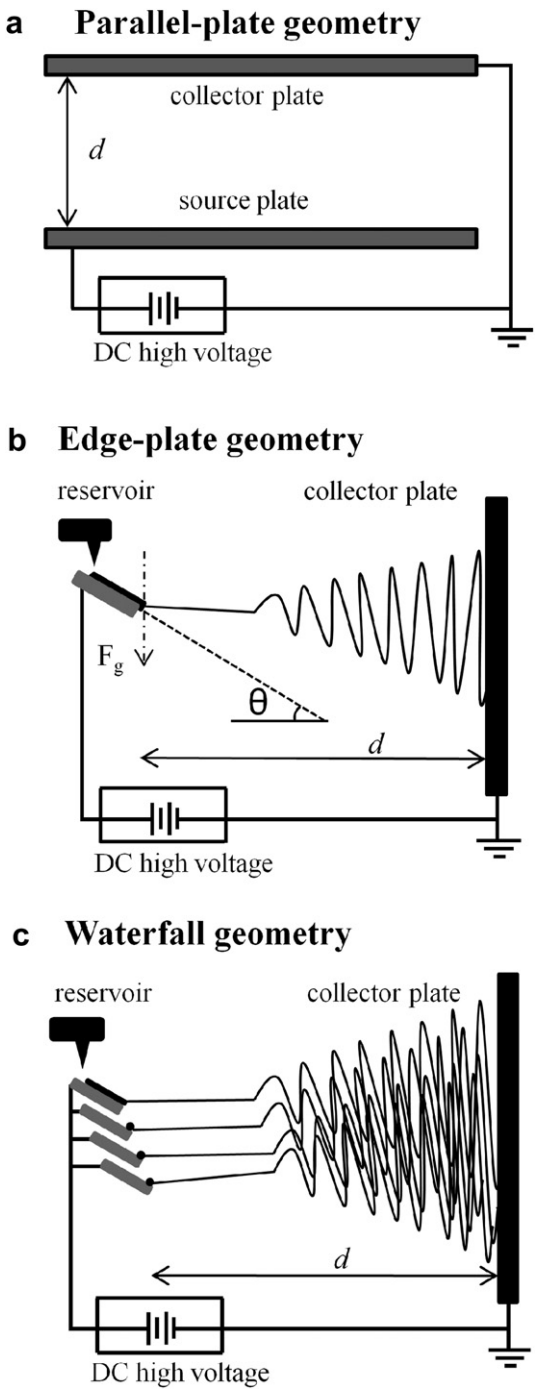

Fig. 3. Illustration of electrospinning configurations with the source-collector working distance d as shown for (a) parallel-plate geometry; (b) edge-plate geometry, with plate angle θ and direction of gravity F_g as indicated; and (c) waterfall geometry.

above the other, separated by a fixed distance (Fig. 3a); the top surface of the lower plate is the source electrode and the bottom surface of the upper plate acts as the collector. The edge-plate configuration consisted of a source plate held at $\theta = 40^\circ$ with respect to horizontal and a vertically oriented (i.e., $\theta = 90^\circ$) collector plate (Fig. 3b). Additionally, multiple source plates (with $\theta = 40^\circ$, plate separation = 0.375", plate overlap = 0.3125") were also stacked to form a waterfall spinning arrangement (Fig. 3c), where each plate is electrically connected to the same high voltage power supply. In all gravity-assisted feed configurations, an electrically insulated reservoir fitted with one or more plastic pipettes supplied polymer solution to the charged plate; each pipette supplied a solution stream that could then serve as a jet initiation site. For the solution utilized, the stream traveled in a straight line from the feed pipette down the plate with little branching. All aluminum source plates were modified with the C_{10} coating as described above.

For edge-plate and waterfall configurations, the polymer flow was gravity-assisted and thus, dependent on the angle at which the plates were held, the volume of the solution in the reservoir, and the size of pipette aperture. For a successful continuous electrospinning process, the polymer flow rate should symmetrically balance the polymer loss caused by the jetting and subsequent nanofiber formation. The presence of excessive fluid volume in the jet initiation region was associated (in the presence of high electric fields) with electrospraying or jet streaming events (where wet solution was propelled directly to the collector). In order to determine the optimal polymer flow, survey experiments were carried out at in the edge-plate configuration for different plate angles from 20° to 70°; the most favorable results were obtained at 40° and this angle was subsequently kept constant throughout the study. Typically, a 50 ml solution was placed in the reservoir and the pipettes had an inner diameter of 1.5 mm. At these conditions, and with a PEO polymer solution zero-shear viscosity of 9250 cP, the flow rate was empirically determined to be 30 μl/min. Typical measurements involved spinning for ~100 min, depleting the reservoir by 3 ml; this small decrease in reservoir fluid was assumed to have minimal effect on the gravity-assisted feed rate. Initial flow rates were also intentionally varied by using larger pipette sizes (2.0 mm diameter for 45 μl/min and 2.3 mm diameter for 55 μl/min).

2.3. Fiber characterization

Nanofiber morphology was studied with a benchtop scanning electron microscope (SEM) (Phenom FEI) operating at 5.0 kV. The samples were coated (Quoron Technologies, S67620) with Au–Pd at a thickness of 100 Å to reduce charging and produce a conductive surface. The SEM images were analyzed using ImageJ Analyzer software to determine nanofiber diameter and mat porosity characteristics; 25 individual measurements made on each sample determined the mean nanofiber diameter and standard deviation. Porosity was quantified by utilizing the gray scale of the SEM images to identify the top layer of fibers and then using image analysis to determine the number of filled (belonging to this first fiber layer) and unfilled pixels.

To characterize the overall quality of the mats produced under different electrospinning conditions and configurations, we define a parameter called spinnability as the relative fraction of the mat which has retained fibrous morphology compared to areas which may be damaged due to incompletely dried fibers or electrospraying. The spinnability is determined by analysis of SEM images of characteristic portions of the mat. For an ideal, stable configuration where no spraying or streaming occurs, spinnability will be maximal (i.e., 100%). Production rates were calculated by electrospinning for 20 min at a known feed rate, determining the resultant mass by weighing the collected mat, and then extrapolating the results to obtain a rate in grams per hour (g/hr).

2.4. Electric field simulations

Electric field distributions for different electrospinning geometries (needle-plate, parallel-plate edge-plate, and waterfall) were modeled using Maxwell SV 2D software. The mesh size was increased until the solution converged. Although a two dimensional analysis of a three dimensional structures has limitations, by considering the symmetry of the arrangements in question, the two dimensional calculation can be viewed as a planar slice through the three dimensional apparatus and therefore, captures the most relevant physical parameters of the design.

3. Results and discussion

3.1. Electric field modeling

We begin with a discussion of electric field strength and homogeneity in different electrospinning configurations. Qualitatively, the TNE electrospinning geometry (needle-plate as depicted in Fig. 1) results in a very inhomogeneous field (Fig. 4a), with the strongest field and field gradient (defined as the rate of change in the magnitude of the electric field along the spinning axis) at the needle tip. Conversely, the parallel-plate geometry (Figs 3a and 4b) results in a homogeneous field near the center of the plates (i.e., no field gradient) and a lower maximum field compared with TNE; however, the sharp edges of the plate can still generate a strong electric field and possess a field gradient. This effect can be emphasized by utilizing the edge-plate geometry (Figs 3b and 4c) where the electric field pattern is now similar to that in TNE, but one could imagine easily forming many spinning sites along the entire edge (emerging out of the surface in Fig. 4c), which may represent a more facile approach to generating parallel spinning sites than employing an array of needles. As discussed later, the electric field gradient at the location of jet formation appears to be a critical parameter to ensure effective jet formation, and this quantity is quite similar in the TNE and edge-plate geometries. Since the strongest gradient tends to occur near the location of the strongest electric field, one goal of this work is to decouple the two effects. It is important to note that while the electric field amplitude is altered by simply adjusting the applied voltage, the electric field gradient is geometry-specific.

These observations can be quantified from the simulation results of each configuration for TNE (Fig. 4a), parallel-plate (Fig. 4b), edge-plate (Fig. 4c), and waterfall (Fig. 4d), respectively. Insets (top right) in each figure are the magnified section of the corresponding boxed area around the particular source electrode. Electric field magnitude at a specific location can be determined using the relevant color scale given for each configuration. For an applied voltage of 15 kV and 15 cm working distance, in the typical TNE geometry the magnitude of the electric field (E) near the needle tip is $4.6 \pm 0.2 \times 10^5$ V/m, gradually decreasing to $7.5 \pm 2.5 \times 10^4$ V/m at the collector. Applying the same voltage and working distance in the parallel-plate geometry, at the center of the source plate $E = 1.0 \pm 0.2 \times 10^5$ V/m and does not vary significantly from that location to the collector, resulting in no electric field gradient. However, the field at the source plate edge ($1.3 \pm 0.1 \times 10^5$ V/m) is higher than that at the center and results in a non-zero electric field gradient. These electric field distributions correspond with other reports of the TNE geometry [40,41] and of unconfined feed electrospinning using cylindrical and disk spinning sources [42]; in particular, the effect of higher field strength at the plate edges can be

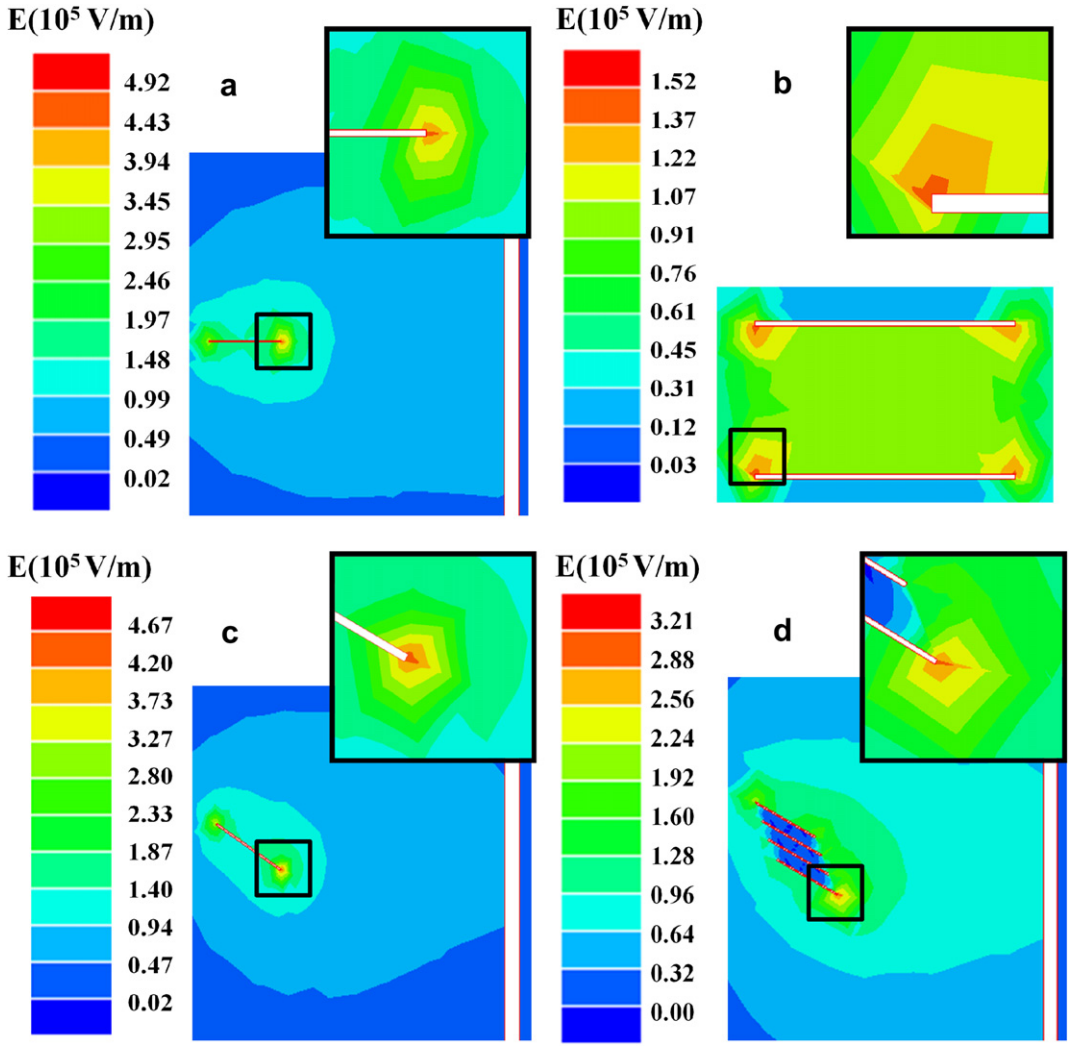

Fig. 4. Simulations of electric field distributions for different configurations with a working distance of 15 cm and an applied voltage of 15 kV: (a) TNE, (b) parallel-plate geometry, (c) edge-plate geometry, and (d) waterfall geometry. Insets are the magnifications of the indicated square areas in each figure.

compared to the cylindrical nozzle edges which displayed a higher magnitude electric field than that at the center of the cylinder.

Fig. 5 compares the change in electric field magnitude with respect to the axial distance away from the spinning locations in the TNE, parallel-plate, and edge-plate configurations. For the parallel-plate configuration, locations at both the plate center and the plate edge were plotted to indicate the effect of the sharp boundary on the electric field magnitude and gradient. This higher electric field and field inhomogeneity generated at the plate's edge can be utilized more efficiently by electrospinning in the edge-plate geometry (Fig. 3b). In this edge-plate orientation, for the same given voltage and working distance, the maximum field is quite similar in magnitude and gradient to that from the TNE configuration given above, (for edge-plate, $4.3 \pm 0.3 \times 10^5$ V/m at the edge and gradually decreasing to $7.5 \pm 2.3 \times 10^4$ V/m at the collector), suggesting that the edge-plate geometry could act as a direct substitute for TNE but with advantage of many more potential spinning sites. However, even though the simulated electric field parameters are comparable, the edge-plate scenario utilizes an unconfined flow of polymer solution over the surface of the plate which alters the jet stability, effective feed rate, and size and shape of the linear and whipping regions, potentially having a deleterious effect on the resultant nanofiber quality. Below we demonstrate

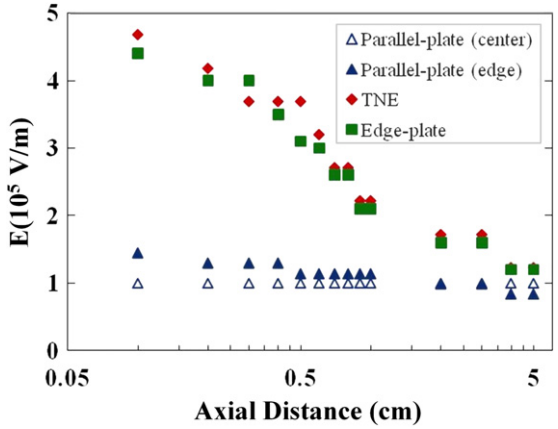

Fig. 5. Graph of electric field magnitude versus axial distance from the spinning site in parallel-plate (triangles, at center (filled) and edge (open)), TNE (diamonds) and edge-plate (squares) configurations.

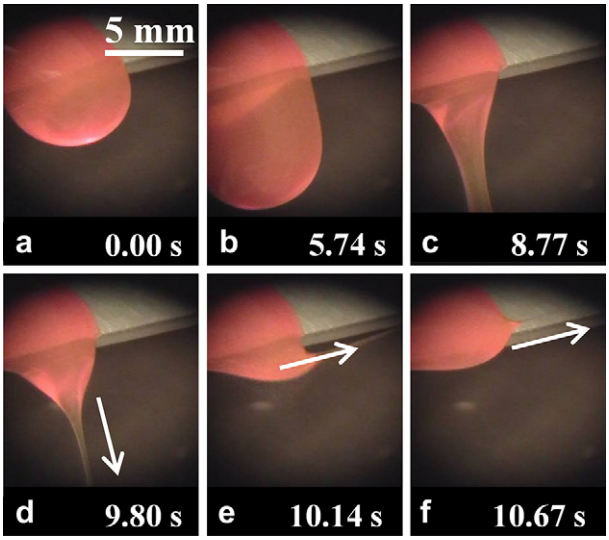

Fig. 6. R6G-tinted PEO solution falling from the source plate, and the subsequent jet initiation process. Sequential images are taken under room light illumination with the time indicated. Arrows in the images (d), (e) and (f) indicate the jet direction. The collector is located towards the right (not shown).

that nanofibers spun from the same solution in TNE and edge-plate configurations in fact can have very similar diameter distribution and average size, yet with the advantage that higher mass throughput is readily obtained when utilizing the edge-plate geometry.

3.2. Jet formation

Experiments in the parallel-plate configuration highlight the importance of the field gradient. Even in the presence of high amplitude fields (up to 40 kV at a 10 cm working distance) and for different sized droplets (5 μl–0.5 ml), no jet initiation was observed from the center of the plate. At this applied voltage, the amplitude of the electric field at the plate center ($4.0 \pm 0.2 \times 10^5$ V/m from simulations) is similar to that close to the needle tip in TNE, but the field is spatially homogeneous – hence, the electric field gradient is essentially zero (in contrast to the TNE case). However when polymer solution was placed near the plate edges, the droplet deformed, jetting occurred, and electrospraying was observed for applied voltages above 30 kV ($d = 10$ cm, effective electric field at the plate edge: $4.5 \pm 0.2 \times 10^5$ V/m from simulations). In order to obtain fibers, we utilized a polymer with a lower solution viscosity and more volatile solvent system (PCL in DCM and DMF). For the PCL solution, (which has a lower viscosity) again no jet formation occurred when droplets were located near the center of the source plate for an applied electric field up to 4×10^5 V/m, however, jetting and nanofiber formation was observed for droplets placed near the plate edges with an applied voltage of 25 kV at a 10 cm working distance (effective electric field $3.8 \pm 0.2 \times 10^5$ V/m). Even when the electric field at the plate center was increased (by raising the applied voltage) to the same magnitude needed for successful spinning from the plate edges, no jetting was observed from the plate center. Summarizing these observations: in regions where the electric field is highly homogeneous (i.e. between plate centers) no jet formation was observed over a wide range of applied electric fields and two different viscosity solutions; in contrast, jet formation was readily seen near the plate edges (where the field varies spatially) for both polymer solutions over a similar range of electric field amplitude values. Therefore, the electric field inhomogeneity (i.e., an electric field gradient) in these regions clearly favors jet formation. Such a hypothesis has previously been proposed [41].

In the edge-plate configuration (Fig. 3b), again jet formation was observed near the plate edge - in particular, where the polymer solution thinned and became a pendent droplet. A typical jet formation sequence is shown in Fig. 6, where for improved imaging contrast, the PEO polymer solution is tinted with a commercial dye. As the polymer solution reaches the edge of the surface treated plate (Fig. 6a), the viscoelasticity of the solution initially maintains the fluid shape (Fig. 6b). Eventually a neck forms (Fig. 6c) and the pendent droplet elongates. The elongation of the fluid (Fig. 6d), combined with the strong electric field and gradient at the plate edge, create conditions for jet self-initiation (Fig. 6e). For a working distance of 35 cm and PEO solutions having a viscosity of 9250 cP, a minimum electric field magnitude at the edge (from simulations) of $4.6 \pm 0.2 \times 10^5$ V/m (corresponding to an applied voltage of 28 kV) was necessary to form the jets. We note that while the magnitude of this electric field is similar to that found in the parallel-plate experiment (where no jet formation was observed) here in addition, the field gradient at the plate edge and the thinning of the polymer solution due to gravity act to aid in self-initiating the stable electrospinning process.

Electrospinning utilizing the edge-plate geometry has both differences and similarities to TNE. In the edge-plate geometry, it is interesting to observe that the Taylor cone is formed on the free surface of the polymer solution (Fig. 6f). Thus, as the fluid flows, the Taylor cone moves dynamically, always apparently forming in the narrowest fluid region and the strongest electric field/field gradient region near the edge of the plate. We refer to such locations as spinning sites. A stable electrospinning process was observed when there was a suitable supply of polymer solution to the given spinning site. Both solution scarcity and excess resulted in extinction and re-creation of the jet, and thus an intermittent rather than continuous electrospinning process. Hence, for gravity-assisted edge-plate geometry, adjustment of the plate angle is another tunable parameter for optimization of stable, continuous electrospinning, analogous to adjusting the feed rate of a syringe pump for optimal TNE.

3.3. Jet profiles

In order to quantify the comparison between TNE and edge-plate electrospinning, Table 1 summarizes the length of the linear region, and the apparent cone angle of the whipping region, comparing jet profiles formed by TNE and edge-plate electrospinning. The apparent cone angle is the densest region of whipping as observed under illumination by a continuous light source.

As shown in Table 1, for a typical configuration, TNE has a small linear region which represents ~22% of the total working distance. We measured the size of the linear region for several different feed rates up to 15 μl/min (Fig. 7, left ordinate) while keeping the electric field and working distance constant. These results are in general agreement with the known trend for TNE [43] that increasing the feed rate enlarges the linear region. Subsequently, the longer linear region effectively reduces the length of the whipping region so the jet spends less time whipping, resulting in larger nanofiber diameters (Fig. 7, right ordinate).

In the edge-plate geometry, the linear region is larger; approximately 28% of the working distance (Table 1). As shown in Fig. 7, the increase in the linear region is due to the higher flow rate; a similar trend is seen in TNE* under comparable parameters (28 kV applied voltage at a working distance of 35 cm, with a larger diameter needle to accommodate greater fluid volume) as a function of feed rate. There are two important observations related to this comparison: First, there is no statistical difference in the length

Table 1
Comparison of electric field values (from simulations) and jet profiles (size of the linear region, and cone envelopes from optical images) from TNE (typical configuration), edge-plate electrospinning, and TNE* (traditional needle electrospinning with the parameters of the edge-plate experiments).

Set Up	Working distance (cm)	Electric Field [V/m]		Linear Region		Whipping Angle
		at tip of the source	near the collector	length (cm)	% of working distance	cone angle (°)
TNE	15	$3.0 \pm 0.2 \times 10^5$	$9.2 \pm 1.5 \times 10^4$	3.3 ± 0.4	22.0 ± 3	48.6
TNE*	35	$4.8 \pm 0.3 \times 10^5$	$6.5 \times 10^4 - 5.1 \times 10^2$	8.3 ± 0.9	23.7 ± 3	26.3
Edge-plate	35	$4.6 \pm 0.3 \times 10^5$	$6.2 \times 10^4 - 3.9 \times 10^2$	9.9 ± 1.2	28.2 ± 4	34.0

of the linear region and the average diameter of the generated nanofibers between the two spinning geometries. Thus, the edge-plate fibers are of the same quality as those produced by TNE under the same feed rate conditions. Second, for TNE*, there is a discontinuous change in the fiber diameter from the TNE arrangement as the spinning parameters are changed to accommodate the higher feed rates (Fig. 8).

3.4. Effect of processing parameters on fiber properties

3.4.1. Fiber diameter and diameter distribution

Fig. 8a (8b) shows an SEM image of electrospun PEO nanofibers obtained from the TNE (edge-plate) geometry. For TNE an average diameter of 243 ± 19.2 nm was obtained with process parameters of 15 cm working distance, 11 kV applied voltage, and a feed rate of 5 μl/min. Utilizing the same polymer solution, a 35 cm working distance, an applied voltage of 28 kV, and a gravity-assisted feed rate of 30 μl/min, edge-plate electrospinning produced nanofibers with an average diameter of 275 ± 32 nm. Thus the mean diameter of the edge-plate electrospun fibers is ~10% larger and the standard deviation is slightly broader than for the optimized TNE process. As discussed in Section 3.3, higher feed rates increase the linear region and correspondingly, decrease the whipping region, resulting in generation of fibers with larger diameter. When edge-plate fibers are compared to those generated by TNE* (i.e., fabricated under similar processing parameters of a 35 cm working distance, 28 kV applied voltage, and a 30 μl/min feed rate) the resulting nanofibers have an average diameter of 292 ± 28 nm within the error of those for the edge-plate electrospun fibers. These results suggest that the principal reason for the increase in the average fiber diameter in this case is the elevated feed rate.

In previous work [14,42,44] where PEO and other polymer nanofibers were electrospun using different unconfined geometries, average fiber diameters were in the range of 200–800 nm with very large standard deviations. It was reported [42] that larger fiber distribution in an unconfined geometry using a cylindrical source was due to the difference in the electric field magnitude at the edges and center of the cylinder which produced finer and coarser fibers respectively. As discussed above, our results imply another reason to account for larger fiber diameter and distribution could be higher feed rate.

Applied voltage and working distance (from 25 to 45 cm) did not have a significant effect on the fiber diameter in the edge-plate configuration. In particular, for three working distances (25 cm, 35 cm and 45 cm) and three average electric field strengths

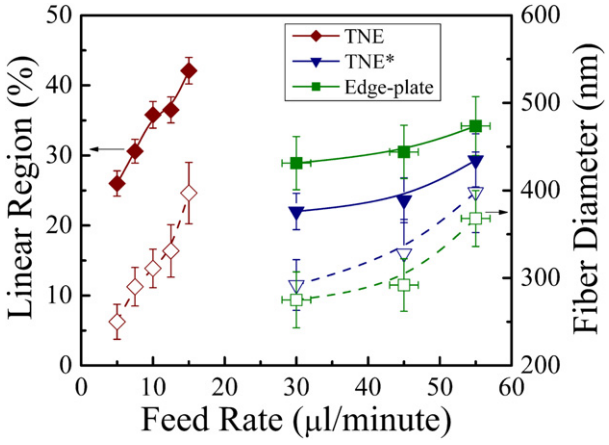

Fig. 7. Length of the linear region (closed symbols, left ordinate) and fiber diameter (open symbols, right ordinate) versus feed rate for TNE (15 cm working distance, 11 kV), TNE* (35 cm working distance, 28 kV) and edge-plate (35 cm working distance, 28 kV) configurations.

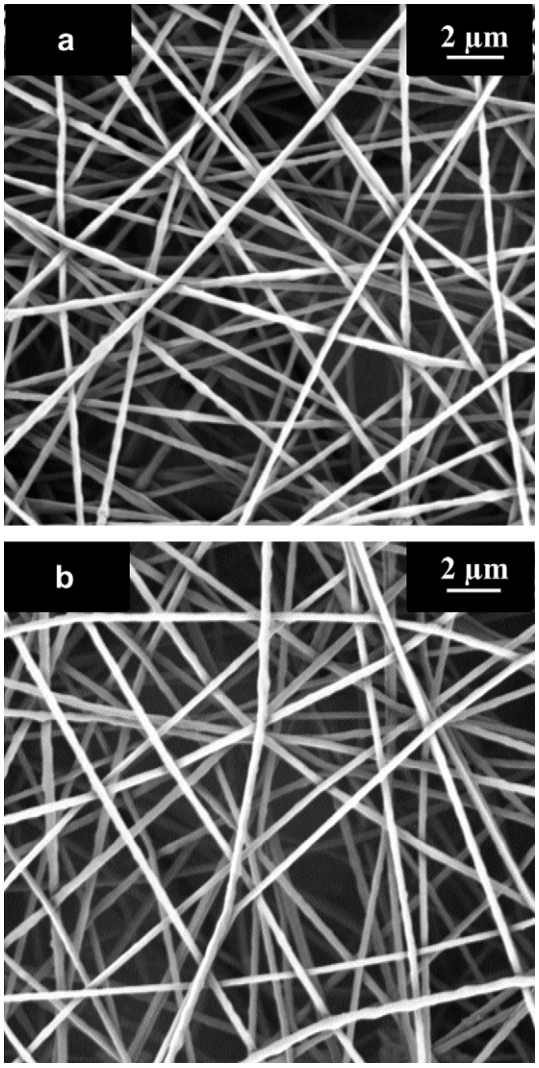

Fig. 8. Comparison of electrospun nanofibers from (a) TNE (15 cm working distance and 11 kV applied voltage) and (b) Edge-plate geometry (35 cm working distance and 28 kV applied voltage).

Table 2
Average fiber diameter and fabrication rate for multiple streams within a single edge-plate configuration. For comparison, values for extended traditional needle electrospinning (TNE*) are included in the first row. For all experiments, the collection time was 20 min under the process conditions of 35 cm working distance, 28 kV applied voltage, and 30 μl/min feed rate (per stream).

# of streams	Center-to-Center Distance Between Pipettes (cm)	Average Nanofiber Diameter (nm)	Fabrication Rate (g/hr)
TNE*	–	292 ± 29	0.11
1	–	275 ± 32	0.13
2	4.8	278 ± 28	0.24
3	2.4	290 ± 41	0.27
5	1.2	311 ± 54	0.19

(9.1×10^4 V/m, 1.0×10^5 V/m and 1.1×10^5 V/m), a slight trend upward in fiber diameter with increased applied electric field, and decreasing diameter with increased working distance, were smaller than the standard deviation of the distribution (~30 nm) (data not shown). Previous work with TNE [25,44–47] and in needle-less electrospinning [42,44] similarly reported that the fiber diameter of electrospun materials was not significantly affected by the applied electric field, consistent with these results from edge-plate spinning.

3.4.2. Spinnability and porosity

We obtained 100% spinnability in both typical TNE (up to a 12.5 μl/min feed rate with 15 cm working distance and 11 kV applied voltage) and edge-plate configurations (up to a 45 μl/min feed rate with working distance 35 cm and 28 kV applied voltage). In the edge-plate geometry, when increasing the feed rate to 55 μl/or for shorter working distances (25 cm), wet solution arrived at the collector, damaging portions of the mat. This was also true for TNE, at high feed rates (>12.5 μl/min at a 15 cm working distance and 11 kV applied voltage). Intermittent spinning (the periodic extinction and re-formation of the jet) was also associated with solution streaming directly to the collector, particularly during jet formation. Thus low spinnability is not intrinsic to unconfined systems, but rather related to high feed rates, short working distances, and/or unstable jet formation in any configuration. Even with these issues spinnability was >95% in most edge-plate experiments.

The porosity of typical TNE electrospun mats was 64.5 ± 3.0% (at a working distance of 15 cm and an average electric field of 7.3×10^4 V/m); edge-plate electrospun mats exhibited higher values of 70.1 ± 4.2%, 71.2 ± 4.8%, and 74.2 ± 4.7% for working distances 25, 35, and 45 cm, respectively (all having an average electric field of 8.1×10^4 V/m). TNE* fibers electrospun at a longer working distance (35 cm) with the same average electric field resulted in a mat porosity of 70.0 ± 3.0%. The diameter of the deposition area for the fibrous mat collected on the grounded plate was found to be approximately 6.5, 14 and 18 cm for TNE (working distance 15 cm, applied voltage 11 kV), TNE* (working distance 35 cm, applied voltage 28 kV) and edge-plate (working distance 35 cm, applied voltage 28 kV) configurations, respectively. We attributed the different between TNE and edge-plate to the longer working distance; this hypothesis is supported by the results from TNE*. Hence, the overall porosity of the nanofibrous mats increases as the working distance increases.

3.4.3. Effect of multiple feed streams on morphology and production rate

In addition to spinning from a single feed source (i.e., a single fluid stream), multiple parallel fluid streams can also be readily utilized in the edge-plate geometry. Table 2 summarizes the results from edge-plate electrospinning under the process conditions of 35 cm working distance, 28 kV applied voltage, and 30 μl/min feed rate per stream. We intentionally located all the spinning sites far from the corners of the source plate in order to have consistent electric field magnitudes and gradients for each stream. The fabrication rate in each case was calculated by extrapolating the results from a 20 min test experiment.

In order to compare with the TNE process, a similarly-timed experiment was conducted under optimal TNE conditions using a 15 cm working distance, 11 kV applied voltage, and a 5 μl/min feed rate, resulting in average nanofiber diameters of 243 ± 19.2 nm with a fabrication rate of 0.027 g/hr. We note, in general, production rates for TNE are in the range of 0.01–0.1 g/hr [11]. From Table 2, it is shown that fabrication rate of edge-plate (with a single fluid stream) is approximately 5× greater than TNE, due, at least in part, to the increased feed rate. This can be confirmed by comparing with TNE* (first row of Table 2). In that case, when the feed rates for both needle and plate electrospinning are matched, plate electrospinning provides a similar, but slightly higher, production rate with a similar, but slightly lower, fiber diameter. Spinnability was 100% for both cases.

In these experiments, increasing the number of feed streams increased the fabrication rate but not in a linear manner. For instance, for three feed streams (where the center-to-center distance is 2.4 cm) the jet from center of the plate was intermittent and thus did not contribute substantially to the production rate. Such sporadic spinning caused streaming of solution directly to the collector (reducing spinnability) and an increased diameter distribution. This observation suggests that intermittent spinning is related to broader diameter distribution. Under these un-optimized spinning conditions, we also observed coalescence of neighboring feed streams, effectively increasing the flow rate to particular spinning sites and resulting in dripping and intermittent spinning.

3.5. Electrospinning from multiple source plates

An alternative and complementary approach to multiple streams is to utilize multiple source plates, for instance in an overlapping, stacked waterfall configuration (Fig. 3c). We conducted several proof-of-principle experiments with different combinations of vertically separated plates (up to four plates) and utilizing multiple feed streams (up to three streams, with spacing 2.4 cm, as mentioned in Section 3.4.3). The plates were held at identical voltages, with a feed rate of 45 μl/min per stream. In this configuration, multiple potential spinning sites were present on each of the four plates. However, the jets were more stable and continuous from the plate with its edge nearest the collector (in this case, the bottommost plate in Fig. 3c). Simulation results help to explain this observation, showing that this spinning site has the highest electric field magnitude/gradient (magnitude: $4.3 \pm 0.2 \times 10^5$ V/m) compared to the other plate edges (magnitude: $2.8 \pm 0.2 \times 10^5$ V/m). The field strength at the collector was $8.3 \pm 1.7 \times 10^4$ V/m for an applied voltage of 32 kV.

Due to the larger flow rate needed to source multiple plates, intermittent spinning was common in the waterfall configuration: the jet initiated within a pendent droplet, a period of continuous electrospinning followed, jet termination occurred due to subsequent flow of polymer solution, and finally the jet re-initiated from a new pendent droplet. Spinning sites on the bottommost plate edges, having a strong electric field and gradient, displayed a reproducible, relatively-long spinning cycle with ~15 s of continuous spinning with ~2 s gap when the jet was extinguished. On the other hand, at spinning sites where the electric field strength and gradient were relatively weak, jets initiated but vanished before becoming stabilized to continuously spin; in other words, the jet was off more often than it was on. Not surprisingly, optical image analysis of the jets formed from spinning sites at the

bottommost plate edges displayed profiles similar to that of the single edge (due to the comparable electric field magnitude and gradient as the single edge-plate) but the jets from other spinning locations manifested shorter linear regions (~20%) and a smaller apparent whipping cone (~30°). These variations and the higher feed rate, contribute to the larger average fiber diameter and wider diameter distribution (290 ± 54 nm) produced under the waterfall configuration for a working distance of 35 cm and 28 kV applied voltage. Spinnability and porosity were found to be 96.0% and 69.0 ± 3.0%, respectively.

To better understand the intermittent electrospinning effect on the nanofiber quality, we mimicked a similar cycle (15 s of spinning with a 2 s gap interval) under TNE* at 28 kV applied voltage, a 35 cm working distance, and a 30 μl/min feed rate. We obtained nanofibrous mats with wet regions (i.e., less than 100% spinnability), caused by jet streaming. The fiber diameter was found to be 325 ± 40 nm, higher than that for the continuous TNE* process (with all other parameters the same) of 292 ± 28 nm. Hence, the increase in the fiber diameter and diameter distribution (i.e., reduction of fiber quality) for the multiple-plate spinning configuration can be attributed to intermittent spinning.

In the waterfall configuration experiments, four plates and three feed streams (offering 12 potential spinning sites) were employed; however at any given instance, only ~4 spinning sites were typically active. Fabrication rate for this configuration was 0.153 g/hr, which is lower than that produced by a two fluid stream feed for a single edge-plate spinning source (Table 2). These results suggest that investigating novel geometries which provide multiple spinning sites on a single edge-plate, or focusing on determining an optimal plate-to-plate overlap and separation that provide identical electric field magnitude and gradients for all plate edges, would be productive research pathways to pursue.

4. Conclusions

In this work we demonstrate a new and simple electrospinning configuration, the edge-plate geometry, which can be straightforwardly implemented for fabricating high quality nanofibers from unconfined fluids. Our results indicate that the local electric field gradient at the spinning site is more significant than the absolute electric field magnitude in order to successfully self-generate a jet, and that the edge-plate geometry has a similar electric field pattern as that in traditional needle electrospinning (TNE). Likewise, the fundamental physical processes underlying edge-plate electrospinning are remarkably similar to that of TNE in terms of the behavior of the linear and whipping regions, and the properties of nanofibrous mats generated under the two configurations are comparable in fiber diameter, diameter distribution, and porosity. When utilizing a single spinning site, we have established that the fabrication rate of edge-plate is approximately 5× higher than that in optimized TNE and similar to TNE* (needle electrospinning with the same processing conditions as edge-plate) but without the possibility of clogging. Thus this simple, unconfined electrospinning configuration provides very similar (if not superior) fiber quality and fabrication rate as needle electrospinning, suggesting a promising pathway towards scaling-up nanofiber production.

Acknowledgements

This work was funded by the National Science Foundation (CMMI #0800237). The authors thank Hai Bui for assistance in fabricating the electrospinning apparatus, Kelly Stano Mulholland for preliminary work on the electric field simulations, and Judy Elson for her assistance with SEM measurements.

References

[1] Ramakrishna S, Fujihara K, Teo W, Lim T, Ma Z. An introduction to electrospinning and nanofibers. Singapore: World Scientific Publishing; 2005.
[2] Formhals A. Process and apparatus for preparing artificial threads. US Patent. 1,975,504; 1934.
[3] Reneker DH, Chun I. Nanotechnology 1996;7(3):216–23.
[4] Kenawy ER, Bowlin GL, Mansfield K, Layman J, Simpson DG, Sanders EH, et al. Journal of Controlled Release 2002;81(1–2):57–64.
[5] Li D, Wang Y, Xia Y. Nano Letters 2003;3(8):1167–71.
[6] Theron A, Zussman E, Yarin AL. Nanotechnology 2001;12:384–90.
[7] Filatov Y, Budyka K, Kirichenko V. Electrospinning of micro- and nanofibers: fundamentals and applications in separation and filtration process. USA: Begell House, Inc. 2007.
[8] Schiffman JD, Schauer CL. Polymer Reviews 2008;48(2):317–52.
[9] McCullen SD, Ramaswamy S, Clarke LI, Gorga RE. Wiley Interdisciplinary Reviews-Nanomedicine and Nanobiotechnology 2009;1(4):369–90.
[10] Tiwari MK, Yarin AL, Megaridis CM. Journal of Applied Physics 2008;103 (4):004305-1–044305-10.
[11] Dosunmu OO, Chase CG, Kataphinan W, Reneker DH. Nanotechnology 2006;17(4):1123–7.
[12] Zhou F, Gong RH, Porat I. Polymer International 2009;58(4):331–42.
[13] Jirsak O, Sanetrnik F, Lukas, D, Kotek V, Martinova L, Chaloupek J. A method of nanofibres production from a polymer solution using electrostatic spinning and a device for carrying out the method. CZ Pat. WO/2005/024101; 2005.
[14] Yarin AL, Zussman E. Polymer 2004;45(9):2977–80.
[15] Wang X, Niu H, Lin T, Xungai W. Polymer Engineering and Science 2009;49 (8):1582–6.
[16] Zhou F, Gong R, Porat I. Journal of Materials Science 2009;44(20):5501–8.
[17] Theron SA, Yarin AL, Zussman E, Knoll E. Polymer 2005;46(9):2889–99.
[18] Fang D, Chang C, Hsiao BS, Chu B. Polymeric Nanofibers; 2006:91–105.
[19] Tomaszewski W, Szadkowski M. Fibres & Textiles in Eastern Europe 2005;13 (4):22–6.
[20] Kim HY. A bottom-up electrospinning devices, and nanofibers prepared by using the same. CZ Pat. WO/2005/0073441; 2005.
[21] Kim HY, Park JC. Conjugate electrospinning devices, conjugate nonwoven and filament comprising nanofibers prepared by using the same. CZ Patent. WO/2007/035011; 2007.
[22] Yamashita F, Ko F, Miyake H, Higahiyama A. Sen-I Gakkaishi 2008;64(124): 24–8.
[23] Kim G, Cho YS, Kim WD. European Polymer Journal 2006;42(9):2031–8.
[24] Bowman J, Tayor M, Sharma V, Lynch A, Chadha S. Materials Research Society Symposiums Proceedings 2003; 752AA1.5.1–AA1.5.5.
[25] Yang Y, Jia Z, Li Q, Hou L, Gao H, Wang L. 8th International Conference on properties and applications of dielectric materials, IEEE transactions on dielectrics and electrical insulation. 2006; 13580–13585.
[26] Yamashita Y, Ko F, Tanaka A, Miyake H. Journal of Textile Engineering 2007;53 (4):137–42.
[27] Vaseashta A. Applied Physics Letters 2007;90:093115.
[28] Paruchuri S, Brenner MP. Physical Review Letters 2007;98(13):134502.
[29] Varabhas JS, Chase GG, Reneker DH. Polymer 2008;49(19):4226–9.
[30] Varesano A, Carletto RA, Mazzuchetti G. Journals of Materials Processing Technology 2009;209(11):5178–85.
[31] Andray AL, Ensor DS, Newsome RJ. Electrospinning of fibers using a rotatable spray head. US Patent. 228,435; 2006.
[32] Srivastava Y, Marquez M, Thorsen T. Journal of Applied Polymer Science; 2007:1063171–8.
[33] Salem DR. Electrospinning of nanofibers and the charge injection method. Nanofibers and nanotechnology in textiles. Cambridge: Woodhead Publishing; 2007.
[34] Lukas D, Sarkar A, Pokorny P. Journal of Applied Physics 2008;103:084309.
[35] Liu Y, He J. International Journal of Nonlinear Sciences and Numerical Simulations 2007;8(3):393–6.
[36] Weitz RT, Harnau L, Rauschenbach S, Burghard M, Kern K. Nano Letters 2008;8 (4):1187–91.
[37] Ulman A. An introduction to ultrathin organic films: from Langmuir-Blodgett to self-assembly. Boston: Academic Press; 1991.
[38] Scott MC, Stevens DR, Bochinski JR, Clarke LI. ACS Nano 2008;2 (11):2392–400.
[39] Shenhar R, Norsten TB, Rotello V. Introduction to nanoscale science and technology. Springer Science Business Media, Inc; 2004.
[40] Kong CS, Lee TH, Lee SH, Kim HS. Journal of Materials Science 2007;42 (19):8106–12.
[41] Yang Y, Jia Z, Liu J, Li Q, Hou L, Wang LM, et al. Journal of Applied Physics 2008;103. 104307–1 – 104307–11.
[42] Niu H, Lin T, Wang X. Journal of Applied Polymer Science 2009;114 (6):3524–30.
[43] Reneker DH, Yarin AL. Polymer 2008;49(10):2387–425.
[44] Cengiz F, Krucinska I, Gliscinska E, Chrzanowski M, Goktepe F. Fibres & Textiles in Eastern Europe 2009;17(1):13–9.
[45] Theron SA, Zussman E, Yarin AL. Polymer 2004;45(6):2017–30.
[46] Tan SH, Inai R, Kotaki M, Ramakrishna S. Polymer; 2005:466128–34.
[47] Wang T, Kumar S. Journal of Applied Polymer Science 2006;102(2):1023–9.